Unravelling Heterodyne Force Microscopy

Verbiest, G.J.

CHAPTER 3

Cantilever Dynamics in Heterodyne Force Microscopy

Heterodyne Force Microscopy showed the possibility to image deeply buried nanoparticles below a surface. However, the contrast mechanism and the motion of the cantilever, which detects the subsurface signal, are not yet understood. We present a numerical study of the cantilever motion in different HFM modes using realistic tip-sample interactions. The results provide information on the sensitivity to the heterodyne signal. The parameters in our calculations are chosen as closely as possible to the situation in real experiments to enable (future) comparisons based on our predictions. In a HFM both the tip and the sample are excited at slightly different ultrasonic frequencies such that a difference frequency is generated that can contain subsurface information. We calculate the amplitude and phase of the difference frequency generated by the motion of the cantilever. The amplitude shows a local maximum in the attractive Van-der-Waals regime and an even higher plateau in the repulsive regime. The phase shifts 180 degrees or 90 degrees, depending on the mode of operation. Finally, we observe oscillations in both the amplitude and the phase of the difference frequency, which are caused by a shift of the resonance frequency of the cantilever and an involved transient behavior.

Most of this chapter is published in [42]

3.1 Introduction

In an HFM, both the sample and the cantilever are excited at slightly different ultrasonic frequencies. The amplitude and the phase of the (nonlinear) difference frequency of the two ultrasonic frequencies allow to extract possible subsurface information at an experimentally accessible frequency. A striking resolution has been reported by Shekhawat and Dravid [6]. Cantrell et al. [8] showed an amplification of the difference frequency signal, when tuning the difference frequency to a contact resonance. This was later applied in an intermitted contact setup by Cuberes [13], where feedback was performed on the fundamental mode of the cantilever while the difference frequency was matched to the frequency of the second cantilever mode. Recently, Tetard et al. introduced Mode Synthesizing Atomic Force Microscopy (MSAFM), in which the nonlinear tip-sample interaction generates a series of frequencies and not only a signal at the difference frequency [14]. Applications of MSAFM focus on measuring hard structures within soft (bio-)materials [9–12].

Until now there is a clear lack of quantification of subsurface measurements. In order to obtain quantitative measurements, one needs to understand both the high-frequency wave propagation in the sample as well as the cantilever dynamics in the vicinity of a vibrating sample, as the latter provides the measurable signal containing the possible subsurface information.

Regarding the wave propagation, it has been shown recently that the high-frequency acoustic excitations in the sample are Rayleigh scattered by subsurface voids or defects (see Chap. 2 or [28]), as the wavelength of ultrasound is on the order of a few millimeter. It has been shown that the expected amplitude contrast is in the order of 10^{-4} times the amplitude of the non-scattered wave; a value so small that its experimental detection is doubtful. However, it has also been shown that the typical phase contrast is in the order of a few millidegrees, which ought to be detectable. Since the phase contrast of a buried particle may be measured more easily than its amplitude contrast, we will also pay attention to the phase of the cantilever motion.

Concerning the cantilever dynamics, it is still not known how a vibrating cantilever reacts to (high-)frequency vibrations of the sample, although the effect on a *static* cantilever has been investigated [43–47]. Since the tip-sample interaction is nonlinear, unexpected effects might occur that could perhaps lead to an increase of the detected amplitude/phase contrast. The nonlinear interaction between the tip and the sample causes the cantilever to vibrate at any frequency, which is a linear combination of the high ultrasonic frequencies through the tip and the sample. Recent work by Cantrell et al. [32] has shown analytically that the phase of the sample corresponds 1-to-1 with the phase of the difference frequency. They make a mode expansion of the motion of the cantilever, in which each mode represents a resonance of the cantilever. This

is analogous to our approach, which we describe in this chapter, except we numerically solve the equation of motion to take into account the full nonlinearity of the tip-sample interaction.

The latest experiments and calculations [33, 48] show that the excitation of the difference frequency is optimal when the cantilever is vibrated in the attractive regime of the tip-sample interaction, where the Van-der-Waals force is dominant. These papers also show that the excitation of the difference frequency is enhanced, if one, in addition, weakly excites the first resonance of the cantilever. However, in their analytical model, it is not possible for the cantilever to indent into the sample. This is an important point, as one would expect the snapping in-and-out of contact with the sample to be the "biggest" nonlinearity that, therefore, produces the strongest signal at the nonlinear difference frequency.

In this chapter we study the cantilever dynamics in Subsurface-AFM. We include the possibility of soft samples and find that the maximum excitation of the difference frequency is in full contact with the sample. The surface of the sample is assumed to vibrate at an ultrasonic frequency (ω_s) with a fixed amplitude (A_s) and phase (ϕ_s). The cantilever is excited at a slightly different ultrasonic frequency (ω_t) with amplitude (A_t) and phase (ϕ_t). This is analogous to the experimental setups of [3, 6, 7, 9–12, 14, 33]. We calculate the excitation of the difference frequency $\omega_{\text{diff}} = |\omega_s - \omega_t|$ as a function of the tip-sample distance (see Fig. 3.1).

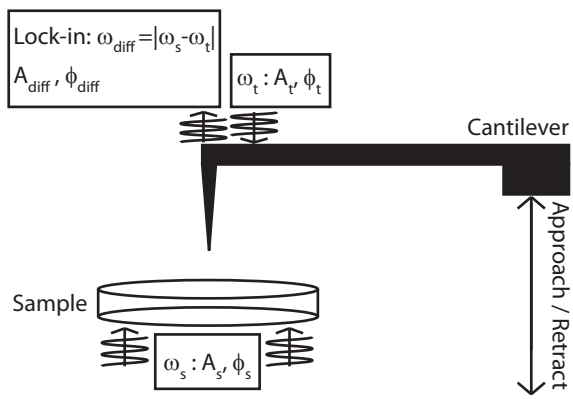

Figure 3.1: The corresponding HFM setup of our numerical calculations. The sample is excited at a frequency (ω_s) with a fixed amplitude (A_s) and phase (ϕ_s), and the cantilever is excited at a frequency (ω_t) with amplitude (A_t) and phase (ϕ_t). The amplitude (A_{diff}) and the phase (ϕ_{diff}) of the difference frequency $\omega_{\text{diff}} = |\omega_s - \omega_t|$ is detected via a lock-in. During approaching and retracting the cantilever from the surface, only the z-position of its base is moved.

We confirm the peak in the Van-der-Waals regime published by Tetard et al. [33], but, in addition, we find that the amplitude of the difference frequency converges to a plateau in the repulsive regime of the tip-sample interaction. Furthermore, we find changes in the phase of the difference frequency that are related to tapping mode operation as well as the sign of the effective drive force at the difference frequency. Finally, we show that there is an excitation of the fundamental resonance (1^{st} mode) of the cantilever, if the cantilever moves in or out of contact with the sample. We discriminate two effects. Firstly, while going in or out of contact, due to its deflection, the cantilever's tip slows down or accelerates, respectively, which results in an excitation of the fundamental resonance of the cantilever. Secondly, in the case that the difference frequency is tuned to the frequency of the 1^{st} mode of a free cantilever, the actual resonance frequency of the cantilever shifts due to the tip-sample interaction. This results in a transient behavior of the oscillator leading to oscillations in both the amplitude and the phase of the difference frequency.

3.2 Theory and Calculation

The dynamics of a cantilever with uniform cross section, fixed on one end and with external forces applied to its free end, is well modelled using the Euler-Beam equation [32, 49, 50], which we, therefore, also take as our starting point.

$$EI\frac{\partial}{\partial x^4}\left[\Phi(x,t)+a_i\frac{\partial\Phi}{\partial t}\right]+\rho wh\frac{\partial\Phi}{\partial t^2} + a_h\frac{\partial\Phi}{\partial t}-\delta(x-L)\left[F_{ts}(z)+F_{drive}(t)\right]=0 \tag{3.1}$$

, in which E is the Young's modulus of the cantilever, I is the moment of inertia, a_i is the internal damping coefficient, ρ is the density, w, h, and L are, respectively, the width, height, and length of the cantilever, a_h is the hydrodynamic damping, $\delta(x-L)$ is the δ-function which describes that the force acts at the free end only, and $\Phi(x,t)$ is the vertical displacement of the cantilever at position x and at time t. F_{drive} is the drive force on the cantilever at its free end and $F_{ts}(d)$ represents the tip-sample interaction acting on the free end, where z is the tip-sample distance. In our model, the tip-sample distance is given by $z = z_b + \Phi(L,t) + A_s\cos(\omega_s t+\phi_s)$, where z_b is the base position (fixed end) of the cantilever, A_s is the vibration amplitude of the sample, ω_s is the angular frequency of the sample, and ϕ_s is the phase of the sample. $\Phi(L,t)$ is the vertical displacement of the end of the cantilever. In first approximation, this consists of the cantilever deflection δ, the ultrasonic tip motion $A_t\cos(\omega_t t+\phi_t)$, and the real motion at the difference frequency $A_{\text{diff}}\cos(\omega_{\text{diff}}t+\phi_{\text{diff}})$. To enable future comparisons with experiments, we

subtract an offset in z_b such that $z_b = 0$, if the deflection $\delta = 0$ during the approach cycle of the cantilever. This is the border between the attractive and the repulsive regime, at which the *effective* force on the cantilever is zero.

We use the boundary conditions of a free cantilever beam, which is clamped at its base and has a tip of mass M_t at its free end:

$$\begin{aligned} \Phi(0,t) &= 0 \\ \frac{\partial \Phi}{\partial x}(0,t) &= 0 \\ \left[EI \frac{\partial^2 \Phi(x,t)}{\partial x^2} + I_t \frac{\partial^3 \Phi(x,t)}{\partial t^2 \partial x} \right]_{x=L} &= 0 \qquad (3.2) \\ \left[EI \frac{\partial^3 \Phi(x,t)}{\partial x^3} - M_t \frac{\partial^2 \Phi(x,t)}{\partial t^2} \right]_{x=L} &= 0 \end{aligned}$$

(3.3)

, where I_t is the moment of inertia of the tip and L is the length of the cantilever. These boundary conditions introduce a discrete set of solutions such that it is possible to solve Eq. 3.1 by using the ansatz $\Phi(x,t) = \varphi(x)\eta(t)$. By applying the mass-normalized eigenmodes, as described in [51], we are able to make a mode expansion: $\Phi(x,t) = \sum_j \varphi_j(x)\eta_j(t)$, where $\varphi_j(x)$ are the mass-normalized eigenmodes and $\eta_j(t)$ are the corresponding amplitudes. The mass-normalized eigenmodes are given by

$$\varphi_j(x)/\alpha_j = \cos\left(\frac{\lambda_j}{L}x\right) - \cosh\left(\frac{\lambda_j}{L}x\right) \qquad (3.4)$$

$$+ \xi_j \left\{ \sin\left(\frac{\lambda_j}{L}x\right) - \sinh\left(\frac{\lambda_j}{L}x\right) \right\} \qquad (3.5)$$

, where λ_j is the j^{th} positive real root of

$$\begin{aligned} &1 + \cos\lambda\cosh\lambda + \lambda\frac{M_t}{mL}\left(\cos\lambda\sinh\lambda - \sin\lambda\cosh\lambda\right) \\ &- \frac{\lambda^3 I_t}{\rho w h L^3}\left(\cosh\lambda\sin\lambda + \sinh\lambda\cos\lambda\right) \qquad (3.6) \\ &+ \frac{\lambda^4 M_t I_t}{(\rho w h L^2)^2}\left(1 - \cos\lambda\cosh\lambda\right) = 0 \end{aligned}$$

, ξ_j is given by

$$\xi_j = \frac{\sin\lambda_j - \sinh\lambda_j + \lambda_j \frac{M_t}{\rho w h L}\left(\cos\lambda_j - \cosh\lambda_j\right)}{\cos\lambda_j + \cosh\lambda_j - \lambda_j \frac{M_t}{\rho w h L}\left(\sin\lambda_j - \sinh\lambda_j\right)} \qquad (3.7)$$

, and the normalization constant α_j is determined from

$$\int_0^L \frac{\partial^2 \varphi_j}{\partial x^2} \frac{\partial^2 \varphi_r}{\partial x^2} EI dx = \omega_j^2 \delta_{rj} \tag{3.8}$$

, where δ_{rj} is the Kronecker delta and ω_j^2 is the eigenfrequency of mode j, which has a corresponding quality factor Q_j:

$$\omega_j^2 = \left(\frac{\lambda_j}{L}\right)^4 \frac{EI}{\rho w h} \tag{3.9}$$

$$Q_j = \frac{\omega_j}{\frac{a_h}{\rho w h} + a_i \omega_j^2} \tag{3.10}$$

Using the mode expansion in Eq. 3.1 we derive a differential equation for $\eta_j(t)$.

$$\ddot{\eta}_j + \frac{\omega_j}{Q_j}\dot{\eta}_j + \omega_j^2 \eta_j = \varphi_j(L)\left[F_{exc}(t) + F_{ts}(z)\right] \tag{3.11}$$

We use this mode expansion (Eq. 3.11) to numerically solve the equation of motion of the cantilever in the time domain. In order to accurately solve the high-frequency motion of the cantilever used in Subsurface-AFM, we need to include the first 10 eigenmodes of the cantilever. This is significantly higher than the 4 modes used in the calculation of [50]. We use a leap-frog algorithm in combination with a 4^{th} order Runge-Kutta method to find the time evolution of η_j.

For our simulations we assumed a standard Silicon cantilever with a stiffness of 2 N/m, which has its first flexural mode at 73.4 kHz. The cantilever has a length of $L = 230\mu$m, a width of $w = 30\mu$m, a height of $h = 2.7\mu$m, a Young's modulus of $E = 179$ GPa, a Poisson ratio of $\nu = 0.28$, a density of $\rho = 2330$ kg/m^3, an internal damping of $a_i = 4.3 \cdot 10^{-10}$ s, a hydrodynamic damping of $a_h = 5.6 \cdot 10^{-4}$ kg/ms, a tip mass of $M_t = 5.4 \cdot 10^{-15}$ kg, a moment of inertia of the tip of $I_t = 3 \cdot 10^{-22}$ kg m^2, and a tip radius of $R = 5$ nm. The damping coefficients a_i and a_h were chosen to match the measured quality factors, Q, of the fundamental mode of 150 and the second mode of 450.

The discussion so far is valid for any tip-sample interaction, but as recent Subsurface-AFM experiments [3,6,8–11,13,14] focus on the application of soft (bio)materials, we apply the DMT-model [23] to describe the tip-sample interaction between the cantilever and the surface. In the DMT-model the tip can, to a certain extent, indent into the sample. We will also calculate the response of the cantilever using the Bradley model of rigid contact, described in Chap. 4. According to the DMT-model, the force-distance relation is given by

$$F_{ts}(z) = \begin{cases} -\frac{HR}{6a_0^2} + \frac{4}{3}E_f\sqrt{R}(a_0 - z)^{3/2} & \text{if } z < a_0 \\ -\frac{HR}{6z^2} & \text{if } z \geq a_0 \end{cases} \tag{3.12}$$

, where we take the value for Silicondioxide for the Hamaker's constant, which is $H = 8.2 \cdot 10^{-20}$ J. The effective interatomic distance is $a_0 = 0.45$ nm, and E_f is the effective Young's modulus

$$\frac{1}{E_f} = \frac{1-\nu^2}{E} + \frac{1-\nu_s^2}{E_s} \tag{3.13}$$

with the Poisson ratio of the sample of $\nu_s = 0.35$ and the Young's modulus of the sample of $E_s = 179$ GPa of Silicon. We removed the discontinuity in the derivatives of $F_{ts}(z)$ at $z = a_0$ by locally approximating $F_{ts}(z)$ with two quadratic functions: one for $0.8a_0 \leq z \leq a_0$, and one for $a_0 \leq z \leq 1.2a_0$, such that $\partial F_{ts}(a_0)/\partial z = 0$. The other constraint is the continuity of both $F_{ts}(z)$ and its derivative at $z = 0.8a_0$ and $z = 1.2a_0$. The sum of the oscillation amplitudes A_s and A_t is always chosen to be larger than the region where F_{ts} is approximated with the two quadratic functions.

Figure 3.2 shows both the tip-sample force (black) as well as the second derivative of the force (gray) with respect to the tip-sample distance z as a function of the tip-sample distance z. Note that the tip-sample interaction $F_{ts}(z)$ is nonzero at $z = 0$:

$$F_{ts}(z=0) = -\frac{HR}{6a_0^2} + \frac{4}{3}E_f\sqrt{R}a_0^{3/2}\,. \tag{3.14}$$

Note also that the second derivative of the force has two extrema: a positive one in the repulsive Hertzian contact force regime, and a negative one

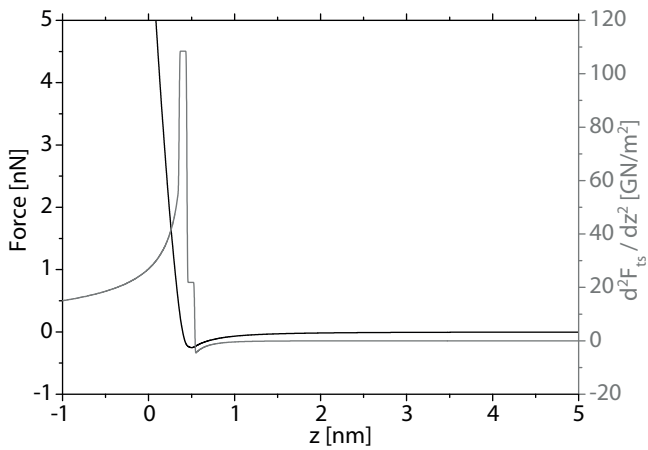

Figure 3.2: The force (black) as a function of the tip-sample distance z. The right scale corresponds to the second derivative of the force (gray) with respect to the tip-sample distance. Note that $F_{ts}(z=0) \neq 0$ per definition (see Eq. 3.12).

in the attractive Van-der-Waals force regime. Also the second derivative is, by choice, constant in between these two extrema.

The reason why we provide the second derivative becomes clear, if one considers the nonlinear (or also called heterodyne) mixing term that mixes the tip vibration with the sample vibration. If we expand the tip-sample interaction with a Taylor series up to second order,

$$\begin{aligned} F_{ts}(z_b+\epsilon) &= F_{ts}(z_b) + \frac{\partial F_{ts}(z_b)}{\partial z}\epsilon + \frac{1}{2}\frac{\partial^2 F_{ts}(z_b)}{\partial z^2}\epsilon^2 \\ \epsilon &= A_s\cos(\omega_s t+\phi_s) + A_t\cos(\omega_t t+\phi_t) \end{aligned} \tag{3.15}$$

one sees that the first term that delivers mixing (multiplication of the two cosines) is given by the third term with a prefactor of the second derivative. The mixing amplitude at the difference frequency is, therefore, a direct function of the second derivative.

Using the force-distance curve of Fig. 3.2, we calculated the cantilever motion as a function of the tip-sample distance to study the nonlinear frequency mixing for the Subsurface-AFM case of a HFM. In the simulation, we start without any tip-sample interaction at 14 nm away from the sample, where we let the cantilever reach its equilibrium motion (with frequency ω_t, amplitude A_t, and phase ϕ_t). Then we turn on the tip-sample interaction and continuously move towards the surface and out again. During this movement, we record the motion of the cantilever, from which we calculate the amplitude (A_{diff}) and phase (ϕ_{diff}) of the difference frequency at $\omega_{\text{diff}} = |\omega_s - \omega_t|$ using a lock-in method.

3.3 Results and Discussion

Following the two different experimental ways of applying the frequencies, as reported in literature [3, 6, 7, 9–12, 14, 33], we also calculated the cantilever response for two different frequency schemes, which we call *off-off resonance* and *on-on resonance* (see also Sect. 1.2 for the different HFM modes).

In the *off-off resonance* scheme all frequencies (that of the tip, the sample, and the nonlinear difference frequency) are far away from any eigenfrequency of the cantilever. We have chosen $\omega_{tip,sample}/2\pi = 0.5\cdot(f_{4^{th}mode} + f_{5^{th}mode} \pm 1\,\text{kHz}) = 0.5\cdot(2.43\,\text{MHz} + 3.90\,\text{MHz} \pm 1\,\text{kHz}) \approx 3.17$ MHz, which leads to a difference frequency of $|\omega_s - \omega_t|/2\pi = 1$ kHz.

In the *on-on resonance* scheme the tip is driven at resonance $\omega_t/2\pi = f_{5^{th}mode} \approx 3.90$ MHz, and the sample frequency $\omega_s/2\pi = f_{5^{th}mode} + f_{1^{st}mode} \approx 3.98$ MHz is tuned such that the difference frequency $|\omega_s - \omega_t|/2\pi = f_{1^{st}mode} = 73$ kHz matches the first eigenmode of the cantilever.

Note that whenever we speak about an eigenfrequency of the cantilever, we refer to the eigenfrequency of the free hanging cantilever not being in contact

with the sample. These eigenfrequencies shift to higher frequencies when the cantilever gets into contact with the sample and shift to lower frequencies in the attractive regime. We denote the amplitude and the phase at the difference frequency with A_{diff} and ϕ_{diff} respectively.

As the shifting of the eigenfrequencies is important for the understanding of this chapter and the rest this thesis, we shortly discuss this issue in the following. The fundamental mode of the cantilever has a resonance frequency of 73 kHz and a spring constant of 2 N/m, if we neglect the tip mass and tip moment of inertia. Because of the tip-sample interaction, the resonance frequency of the cantilever shifts to lower frequencies, when the tip-sample interaction is attractive, and to higher frequencies, when the tip-sample interaction is repulsive [1]. Next to these relatively small shifts, the mode shape changes, if the cantilever gets into full contact with the sample. If the tip-sample contact gets sufficiently stiff, the resonance frequency will become that of the first *contact resonance*, which is $\sim$ 320 kHz for the used cantilever (see also Fig. 5.4). In our simulation, due to the bending of the cantilever, we do not reach sufficient tip-sample stiffness and the first resonance shifts only up to $\sim$230 kHz (the maximum tip-sample stiffness that we reach in all experiments described in this thesis is indicated with a vertical dashed line in Fig. 5.4.). The higher eigenmodes of the cantilever are much stiffer than the 2 N/m of the fundamental mode: the spring constant can go up to several 1000 N/m. As a consequence, the frequency shift of the higher eigenmodes caused by the tip-sample interaction is, therefore, negligible. We estimate the frequency shift of the higher eigenmodes to be $1000[N/m]/2[N/m] \approx 500$ times smaller than the frequency shift of the fundamental mode, which can be read of at the position of the horizontal line for the 5^{th} mode in Fig. 5.4. The contact resonance of the 4th eigenmode, with a resonance frequency of 2.43 MHz, is 3.61 MHz. However, in order to reach this high frequency contact resonance the tip-sample contact has to get 100 times stiffer than in the case of the first contact resonance. This is impossible in our case, as we even do not reach the first contact resonance (see Fig. 5.4). Strictly speaking, one would need an infinitely stiff tip-sample contact to reach the contact resonances. As the fundamental mode shifts towards the contact resonance ($\sim$ 230 kHz), the frequency shift of the 4^{th} eigenmode with 2.43 MHz is only $\sim$ 20 kHz. This, together with the fact that the quality factor, Q, of the 4^{th} eigenmode is 146, implies that A_t and ϕ_t are constant in the *off-off resonance* scheme: the tip indents into the relatively soft sample without significant changes to the cantilever resonance frequency. In the *on-on resonance* scheme the same argumentation is valid; we use the 5^{th} eigenmode of 3.90 MHz, which shifts only $\sim$ 10 kHz during the approach and has a Q of 92. At this point it is important to note that, due to the missing frequency shift of

[1] Actually it is the sign of the first derivative of the force, which matters for the definition of attractive and repulsive interaction.

the high frequency tip motion, also the difference frequency is constant in the *on-on resonance* scheme. The cantilever is driven with a constant (difference) frequency on its fundamental mode. However, when getting into contact, the first mode shifts to the contact resonance, which implies a phase shift of 90 degrees. We will see back this 90 degrees phase shift in our results.

We start with the introduction of the *off-off resonance* results. In Fig. 3.3 the amplitude of the difference frequency for the *off-off resonance* case is plotted as a function of the base position z_b of the cantilever for various A_s, while A_t is kept constant at 1 nm. There is no frequency mixing far away from the surface (the oscillations are an artefact of our lock-in detection). When approaching the sample, we observe a local maximum before the mixing amplitude converges to an even higher plateau in the repulsive regime. The plateau has not been observed before and is complimentary to the work of Tetard et al. [33], who reported about a maximum in the attractive Van-der-Waals regime. The

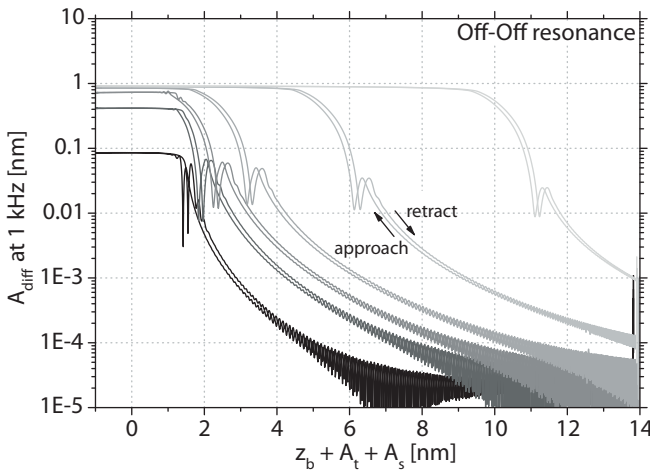

Figure 3.3: The amplitude of the difference frequency for the *off-off resonance* case as a function of the height of the cantilever's base $z_b + A_s + A_t$ (that determines tip-sample distance z). Note that the x-axis is not linear in z due to the involved cantilever deflection δ. $z_b = 0$ defines the border between the attractive and the repulsive regime, at which the *effective* force on the cantilever is zero. A_s is 0.1 nm, 0.5 nm, 1 nm, 2 nm, 5nm, and 10 nm and is color coded from black to light grey. A_t is fixed and equal to 1 nm. The results are symmetric in A_s and A_t: by interchanging the values of A_s and A_t in the simulation, we obtain exactly the same result for the amplitude of the difference frequency. We see a local maximum before the mixing amplitude reaches an even higher plateau. The black arrows indicate the approach and retract curve.

results shown in Fig. 3.3 are symmetric in A_s and A_t: by interchanging the values of A_s and A_t in the simulation, we obtain exactly the same result for the amplitude of the difference frequency (we will show the symmetry in A_s and A_t also analytically in Chap. 5). We will discuss both the local maximum and the plateau later. It is interesting to note that we also find a local maximum and a plateau, when applying a Lennard-Jones potential (see Chap. 4 or [52]).

Investigating Fig. 3.3 more closely reveals that the amplitude of the peak in the attractive Van-der-Waals regime decreases when A_s increases. This implies the existence of an optimal combination of A_t and A_s, which maximizes the peak in the attractive Van-der-Waals regime. We expect that the optimal combination of A_t and A_s is such that only the part of the force-distance curve is probed where the second derivative is maximal: $A_t + A_s \approx 0.1$ nm. In addition, we also observe that the plateau is reached more quickly for smaller A_s. We will come back to this later.

Furthermore, when looking at Fig. 3.3, one immediately notes the hysteresis between the approach and retract curves. This is a numerical effect caused by the way we calculate the force distance curves. The cantilever is moved continuously towards the surface, after which it is moved away from the surface. This continuous movement together with the fact that the cantilever needs some time to adjust the amplitude of the difference frequency (involved Q factor), lets the cantilever feel different effective forces on its way towards the sample with respect to its path away from the sample. In other words, a shift in time equals a shift in z_b position, which leads to the hysteresis. The hysteresis vanishes, if the cantilever approaches the surface infinitely slowly.

In all figures to follow, we have chosen A_s of 0.1 nm and A_t of 10 nm. Also, everything is plotted as a function of the height of the cantilever's base z_b.

Figure 3.4 shows the amplitude of the difference frequency plotted in black and the corresponding cantilever deflection plotted in grey. The dotted vertical line indicates the point, where the repulsive part of the tip-sample interaction is first felt by the cantilever. The mixing strength increases as one approaches the sample, because the Van-der-Waals force is increasing and is nonlinear. As the mixing strength is a direct function of the second derivative of the tip-sample interaction (see above), we expect two maxima [2]: one in the attractive Van-der Waals regime and one in the repulsive regime. This explains the local maximum to the right of the dotted vertical line in Fig. 3.4 indicating that it is in the attractive regime of the tip-sample interaction, which is in agreement with [33]. However, instead of seeing a second maximum, we observe a plateau that is completely caused by the repulsive part of the tip-sample interaction.

At this point one should realize two important facts. First, the spring constant of the 5^{th} eigenmode is in the order of 10^3 N/m whereas the spring

[2] The change in sign of the second derivative of the tip-sample interaction leads to a phase change of the nonlinear mixing frequency.

constant of the fundamental mode is only 2 N/m. Therefore, the cantilever starts bending (resulting in a deflection, see Fig. 3.4) before the tip-sample stiffness reaches a value that is comparable to the stiffness of the 5^{th} eigenmode. As a consequence, the high frequency tip excitation effectively does not feel the sample and maintains its free amplitude A_t. In other words, even if the tip gets into full contact with the sample, the high frequency tip vibration is maintained and the cantilever bends. This explains why we do not observe a second maximum in the repulsive regime. This result is rather unexpected, because experimentally A_t decreases with further indentation into the sample, i.e. in a tapping-mode approach curve of a cantilever driven at its first mode or higher modes the amplitude eventually goes down. The second point to realize is that A_s is constant by choice.

Keeping these two issues in mind, we can understand the different plateau values as a function of the sample amplitude A_s, as visible in Fig. 3.3.

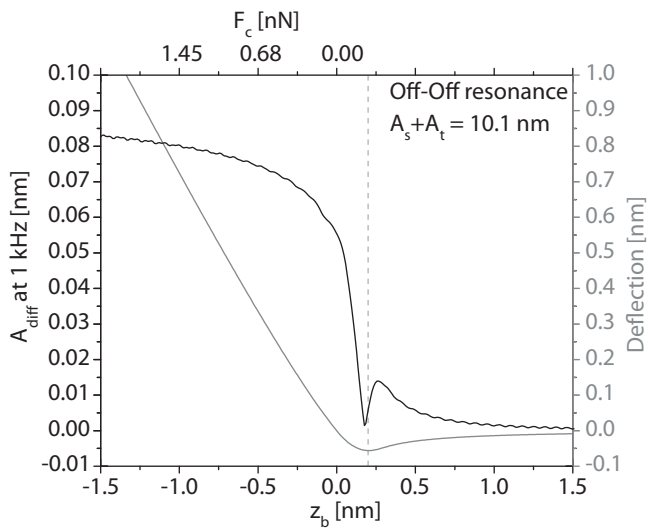

Figure 3.4: The amplitude (black) of the difference frequency and the corresponding cantilever deflection (gray) as a function of the height of the cantilever's base z_b (that determines tip-sample distance z). Note that the x-axis is not linear in z due to the involved cantilever deflection δ. $z_b = 0$ defines the border between the attractive and the repulsive regime, at which the *effective* force on the cantilever is zero. A_s is 0.1 nm and A_t is 10 nm. The dotted vertical line indicates the point where the repulsive part of the tip-sample interaction is first felt by the cantilever. We see that a local maximum of the mixing amplitude is in the attractive Van-der-Waals regime of the tip-sample interaction, whereas an even higher plateau is reached in the repulsive regime.

The cantilever is oscillating in/on a surface, which is vibrating at a slightly different frequency. The sample surface is thus at a different z-position for each high frequency oscillation of the cantilever. This results in a beating (and not nonlinear mixing) of the cantilever's deflection at the difference frequency. The amplitude of the beating is found from the following mathematical identity

$$\begin{aligned} &A_s\cos(\omega_s t+\phi_s)+A_t\cos(\omega_t t+\phi_t)= \\ &\quad\sqrt{A_t^2+A_s^2+2A_tA_s\cos(\omega_{\text{diff}}t+\phi_s-\phi_t)}\times \\ &\qquad\cos\left(\frac{\omega_s+\omega_t}{2}+\frac{\phi_s+\phi_t}{2}+\tan\left\{\frac{A_s-A_t}{A_s+A_t}\arctan\left[\frac{\omega_{\text{diff}}}{2}+\frac{\phi_s-\phi_t}{2}\right]\right\}\right) \\ &\equiv\sqrt{A_t^2+A_s^2+2A_tA_s\cos(\omega_{\text{diff}}t+\phi_s-\phi_t)}g(\omega_h) \end{aligned} \tag{3.16}$$

, where $|g(\omega_h)|\leq 1$ is a harmonic function oscillating at a *single* angular frequency ω_h ($\omega_t\leq\omega_h\leq\omega_s$). The low frequency amplitude of this beating A_{diff}^{max} is derived from Eq. 3.16:

$$A_{\text{diff}}^{max}=A_t+A_s-\sqrt{A_t^2+A_s^2} \tag{3.17}$$

In Tab. 3.1 we compare the simulation values of the plateaus, $A_{plateau}$, derived from Fig. 3.3 with the theoretical values A_{diff}^{max}. We find a very good agreement except for intermediate values of A_t and A_s. The good agreement between A_{diff}^{max} and the values of the plateaus indicates the linearity of the tip-sample interaction deep in the repulsive regime and, therefore, the importance of beating for the generation of the signal at the difference frequency (as will be addresses in detail in Chap. 6). Now we can also understand why the plateau's in Fig. 3.3 are reached earlier for small A_s. With a smaller amplitude A_s, the cantilever is sooner, during the approach, probing only the most nonlinear part of the tip-sample interaction, which effectively results in the plateau, due to beating.

As mentioned above, in experiments we do not observe a plateau. The reasons are the following. Firstly, significant damping between the tip and the sample, especially at high frequencies, ensures that both A_t and A_s decrease and do not remain constant, in contrast to our simulations. Secondly, the sample is also influenced by the tip motion, thereby possibly changing A_s locally. Thirdly, as soon as the tip is indented A_s+A_t, the cantilever is in contact with the sample during the complete ultrasonic motion. As a consequence, the tip-sample interaction approaches a more linear dependence (as it is deeper in the repulsive regime). This implies that the generation of the nonlinear heterodyne signal, A_{diff}, starts to decrease to zero, as $\partial F_{ts}/\partial z$ approaches zero causing also that I_2 in Eq. 5.27 as well as A_{diff} in Eq. 5.24 approach zero. Due to these

three reasons, one expects that the difference amplitude, A_{diff}, decreases to zero for sufficiently deep indentations. This converts the plateau into a second maximum, this time in the repulsive regime. We confirm the decrease of the difference amplitude A_{diff} in Figs. 6.3, 6.12, and 6.14. These figures show that for indentations approximately equal to $A_s + A_t$, the difference amplitude A_{diff} decreases to zero, due to the decrease of I_2 to zero.

A_s [nm]	0.1	0.5	1.0	2.0	5.0	10.0
A_{diff}^{max} [nm]	0.095	0.382	0.586	0.764	0.901	0.950
$A_{plateau}$ [nm]	0.085	0.414	0.729	0.851	0.898	0.913

Table 3.1: The comparison between the theoretical values A_{diff}^{max} for beating and the values of the plateau's, $A_{plateau}$, obtained from the simulation in Fig. 3.3 for different A_s. A_t is fixed and equal to 1.0 nm.

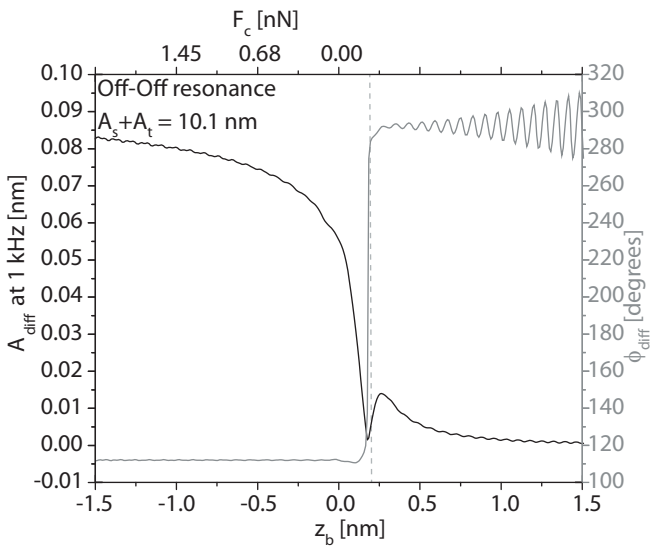

Figure 3.5: The amplitude A_{diff} (black) and the phase ϕ_{diff} (grey) of the difference frequency as a function of the height of the cantilever's base z_b (that determines tip-sample distance z). Note that the x-axis is not linear in z due to the involved cantilever deflection δ. $z_b = 0$ defines the border between the attractive and the repulsive regime, at which the *effective* force on the cantilever is zero. A_s is 0.1 nm and A_t is 10 nm. The dotted vertical grey line indicates the point where the repulsive part of the tip-sample interaction is first felt by the cantilever. We observe a 180 degrees phase shift, when the cantilever gets into contact with the sample.

Figure 3.5 displays the amplitude A_{diff} (black) of the difference frequency with its corresponding phase ϕ_{diff} (grey) for the *off-off resonance* case. Again, the dotted vertical line indicates the point, where the repulsive part of the tip-sample interaction is first felt by the cantilever. The oscillations in the phase for $z > 0.55$ nm are a numerical artifact, as the mixing amplitude is too small for an accurate phase determination.

We observe a phase shift of 180 degrees while approaching the surface and attribute this to a change of the sign of the drive force. In the attractive regime the sample effectively pulls the cantilever towards the surface (at the point of closest approach), whereas in contact the sample pushes the cantilever away. Effectively, this results in a 180 degrees phase shift in the excitation at the difference frequency. Another important observation is that the phase shift of 180 degrees has a certain width: it does not shift instantaneously at a certain z-position. The width increases with increasing amplitudes A_s and A_t of the high frequency vibrations.

Let us now discuss the *on-on resonance* case and compare this with the *off-off resonance* case. Figure 3.6 shows the amplitude of the free fundamental mode (1^{st} resonance) of the cantilever in the *off-off resonance* case (black, lower panel) and A_{diff} at the first resonance in the *on-on resonance* case (grey, upper two panels). In the black line of the *off-off resonance* case, one sees two maxima (approach and retract) that barely stick out over the oscillations of the noise level, which are caused by the error in the amplitude calculation of the lock-in. These maxima occur when, firstly, the cantilever's tip moves into contact and effectively slows down with respect to the overall approach movement and, secondly, when the tip moves out of contact and effectively accelerates during its movement away from the surface to keep up with the overall retract movement. Both, this effectively slowing down and the acceleration of the cantilever, excite resonance frequencies and, therefore, give rise to a shock in the amplitude of the fundamental resonance.

In contrast to the *off-off resonance* case, where the shock barely excites the fundamental mode of the cantilever, the oscillations in the *on-on resonance* case (upper two panels in Fig. 3.6) are real and not caused by the error of the lock-in (please note that the scales differ a factor 100). When approaching the surface, the resonance frequency of the fundamental mode of the cantilever continuously shifts to lower frequencies due to the attractive part of the tip-sample interaction, while the difference frequency remains constant. This leads to a transient behavior of the cantilever motion: the cantilever is driven slightly off resonance, but each period with a different drive phase due to the continuous shifting. The varying drive phase results in an effective decrease or increase of the signal at the difference frequency. The frequency of the oscillation at the difference frequency should be approximately equal to the frequency shift of the resonance frequency. We observe

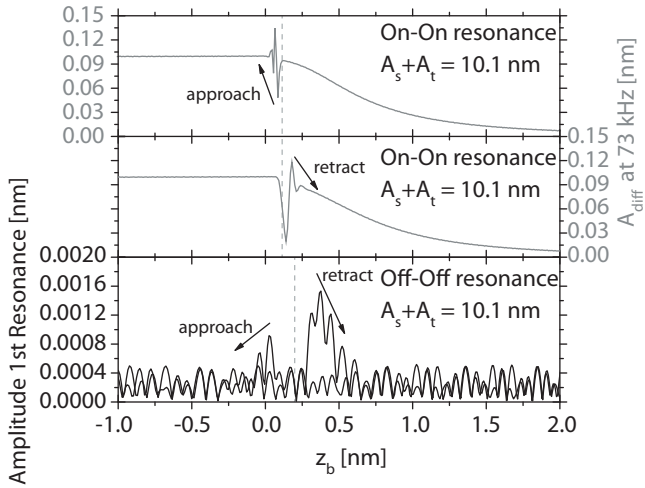

Figure 3.6: The amplitude (black, lower panel) of the fundamental mode of the cantilever in the case of the *off-off resonance* scheme and the mixing amplitude (gray, upper panels) in the case of the *on-on resonance* scheme as a function of the height of the cantilever's base z_b (that determines tip-sample distance z). Note that the x-axis is not linear in z due to the involved cantilever deflection δ. $z_b = 0$ defines the border between the attractive and the repulsive regime, at which the *effective* force on the cantilever is zero. A_s is 0.1 nm and A_t is 10 nm for both curves. The black arrows indicate which oscillations belong to the approach curve and which ones to the retract curve. The correspondence in the z-position between the maxima of the black line and the oscillations of the gray line indicate that the oscillations in the mixing amplitude are related to getting in and out of contact with the surface.

oscillations with a maximum frequency of ∼1.5 kHz, which corresponds to the maximum frequency shift caused by the attractive Van-der-Waals interaction. The time scale, at which these oscillations should damp out, is equal to $Q/\pi f_0 \approx 0.65$ ms, or at our rate of approaching the sample corresponds to 0.02 nm, which is approximately the distance between the peak at $z = 0.40$ nm and $z = 0.38$ nm. We determine the amplitude of the oscillation by taking the average of the peak maximum and the valley to the right of the peak. The amplitude of the peak at $z = 0.40$ is then ≈ 0.043 nm, while the peak at $z = 0.38$ nm has an amplitude of ≈ 0.015 nm. These two amplitudes differ approximately a factor e as one expects. Similar arguments hold for the case where the cantilever is retracted from the surface, which explains the oscillations in the retract curve. In conclusion, the oscillations in the amplitude are a result of the transient behavior of the cantilever, in which it is driven slightly

off resonance.

Let us now focus on the phase ϕ_{diff} of the difference frequency in the *on-on resonance* case, which also shows oscillations as depicted in the lower panel of Fig. 3.7. The upper panel shows the amplitude A_{diff} of the difference frequency as a reference. As discussed above, the cantilever is driven slightly off resonance with a varying drive phase (transient behavior). This variation is, therefore, also reflected in the phase of the difference frequency, resulting in similar oscillations as in the amplitude. In addition, we observe a global 90 degrees phase shift between being far away from the surface and getting into contact. This is in correspondence with an intermitted contact mode (or tapping mode) AFM and is caused by the frequency shift of the

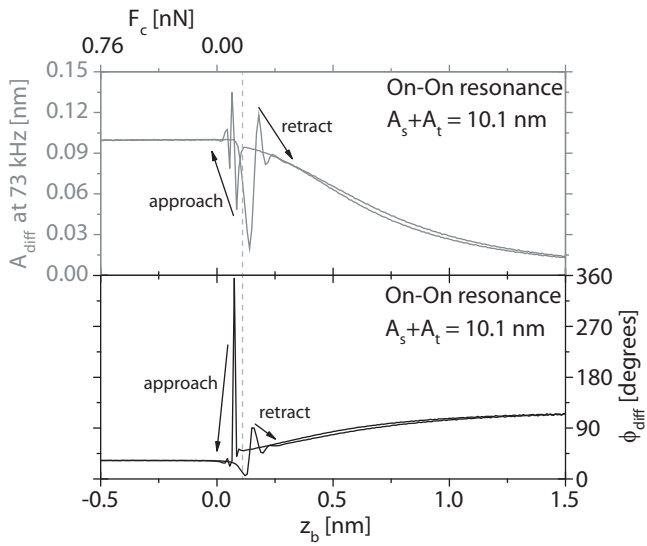

Figure 3.7: The amplitude A_{diff} (gray, upper panel) and phase ϕ_{diff} (black, lower panel) of the difference frequency as a function of the height of the cantilever's base z_b (that determines tip-sample distance z) for the *on-on resonance* excitation scheme. Note that the x-axis is not linear in z due to the involved cantilever deflection δ. $z_b = 0$ defines the border between the attractive and the repulsive regime, at which the *effective* force on the cantilever is zero. A_s is 0.1 nm and A_t is 10 nm. The black arrows indicate which oscillations belong to the approach curve and which ones to the retract curve. Note that the oscillations, which are caused by the shifting of the resonance frequency and the driving of the oscillator slightly off resonance (transient behavior), are observed in both the phase and mixing amplitude. In addition to the oscillations, we observe an overall 90 degrees phase shift between far away from the sample and getting into contact.

fundamental mode of the cantilever: far away from the surface the cantilever is driven at its resonance frequency, which shifts to higher frequencies (see above) when getting into contact thereby changing the phase exactly 90 degrees.

Finally, we stress that in the calculations discussed here the amplitude and phase of the sample vibration are kept constant. In reality, the cantilever might influence and disturb the sample vibration.

3.4 Conclusion

In order to quantify the mixing amplitude and phase in Heterodyne Force Microscopy, which can contain subsurface information, we performed numerical calculations of the response of a cantilever that is vibrating at an ultrasonic frequency ω_t in the vicinity of a sample, which vibrates at a slightly different ultrasonic frequency ω_s, to determine the amplitude and phase of the difference frequency $\omega_{\text{diff}} = |\omega_s - \omega_t|$ as a function of the tip-sample distance. In analogy to reported HFM experiments, we calculated the results for two excitations schemes: the *off-off resonance* scheme and the *on-on resonance* scheme.

In the *off-off resonance* excitation scheme, we have shown that the amplitude of the difference frequency has a local maximum in the attractive Van-der-Waals regime, which is in agreement with [33]. In addition, we have found a plateau in the repulsive regime. This unexpected behavior is the result of two effects. Firstly, the high stiffness of the higher cantilever eigenmodes ensures that A_t is constant: the cantilever bends, thereby leaving the high frequency motion unaltered. Secondly, the constant high-frequency cantilever motion together with the constant high-frequency sample motion causes a beating in the deflection at a low difference frequency, which is smaller than the fundamental mode of the cantilever. The combination of these two effects explains why the height of the plateau is equal to the beating amplitude of the two ultrasonic vibrations with amplitudes A_t and A_s.

Furthermore, we have shown the existence of an optimal combination of A_t and A_s, which maximizes the peak in the attractive Van-der-Waals regime. Also we have shown that the amplitude of the difference frequency reaches the plateau sooner for smaller A_s.

The results of the *on-on resonance* scheme are similar to the results of the *off-off resonance* scheme. In addition, the *on-on resonance* scheme shows oscillations in both the amplitude and the phase of the difference frequency. These oscillations are the result of effectively driving the cantilever slightly off resonance, which leads to a transient behavior of the cantilever. The phase of the effective drive force is varying, resulting in an effective damping or amplification of the signal at the difference frequency. The variations in the drive phase are reflected in oscillations of the phase of the difference frequency.

In the *off-off resonance* excitation scheme, the phase of the difference frequency shows a 180 degrees phase shift when one gets in contact with the

surface. This shift is caused by a change of the sign in the effective drive force at the difference frequency. The width (or z-range), over which this phase shift occurs, increases with increasing amplitudes A_s and A_t of the high frequency signals. In the *on-on resonance* scheme the phase shift is only 90 degrees; it is caused by the frequency shift of the fundamental mode similar to the shift in intermitted contact mode operation.

The presented numerical study sets the stage to understand reported and future HFM measurements, as a quantitative understanding that combines the cantilever dynamics with different tip-sample interactions, is still missing. A study that takes into account both the altered tip-sample interaction above buried nanoparticles and the cantilever dynamics, might explain the reported subsurface contrasts.